Available online at www.sciencedirect.com
SCIENCE DIRECT®
Materials Chemistry and Physics 93 (2005) 181–186
MATERIALS CHEMISTRY AND PHYSICS
www.elsevier.com/locate/matchemphys

Neural computation to correlate HVOF thermal spraying parameters with the magnetic properties of FeNb alloy deposits

M. Cherigui *, S. Guessasma, N. Fenineche, C. Coddet

Laboratoire d'Etudes et de Recherches sur les Matériaux, Les Plasmas et les Surfaces (LERMPS), Université de Technologie de Belfort-Montbéliard (UTBM), Site de Sévenans, 90 010 Belfort Cedex, France

Received 22 January 2005; received in revised form 7 March 2005; accepted 10 March 2005

Abstract

The effect of the HVOF process parameters on coating porosity and magnetic properties of FeNb deposits was studied using artificial neural network methodology. A first artificial neural network was used and optimized to relate process parameters to the magnetic properties of the coating. The effect of process parameters on magnetic properties was quantified by a second network. Predicted magnetic properties correlated with coating porosity were obtained using these optimized network structures. It was then possible to identify the role of porosity with regards to improvement of coercivity and saturation magnetization.

Keywords: Amorphous materials; Coatings; Magnetic properties; Computer modelling and simulation

1. Introduction

Amorphous metallic alloys (often termed metallic glasses) can be produced by rapid quenching from the metallic liquid at sufficient cooling rates to suppress the nucleation and growth of crystalline phases [1,2].

A significant number of alloys are likely to have a non-crystalline structure (amorphous or pseudo-amorphous) when they are solidified at a cooling rate higher than 10^5 K s^{-1}. There has been considerable interest in the manufacture of Fe-based metallic glasses because they permit to obtain attractive combinations of properties such as high hardness and good abrasive wear resistance together with enhanced corrosion resistance and good magnetic properties [1–4].

However, in order to achieve high cooling rates in metallic alloy melts, samples less than 50 μm thick must be suddenly brought into good thermal contact with an efficient heat sink [1–5]. Hence, these amorphous alloys are frequently produced in the form of ribbon or powder.

Thermal spraying has become a very advantageous method that can be used as an alternative approach to deposition of powder material at high deposition rates. Powder particles are injected into a plasma jet, where they are melted and accelerated towards a substrate [6].

In the present study, we have used the high-velocity oxy-fuel (HVOF) thermal spray technique. This process is adequate for spraying low and intermediate melting temperature materials (e.g., polymers and metals). It facilitates high particle velocities needed for amorphization compared to other spray techniques.

In this study, FeNb alloy was chosen as feedstock material for its good tendency for amorphization [7–9]. The literature indicates rather little previous work on the use of such material as a feedstock for thermal spraying.

It is well known that the microstructure, especially grain size, determines the hysteresis loop of a ferromagnetic material [10]. However, other factors can be associated with the degree of softness when using thermal spray technology. Among these factors, coating porosity is regarded as an im-

* Corresponding author. Tel.: +33 3 84 58 32 43; fax: +33 3 84 58 32 86.
E-mail address: mohamed.cherigui@utbm.fr (M. Cherigui).

0254-0584/$ – see front matter © 2005 Elsevier B.V. All rights reserved.
doi:10.1016/j.matchemphys.2005.03.042

portant parameter. The role of this microstructural feature is investigated in this study.

2. Experimental procedure

2.1. Coating preparation

Fe50 wt.% Nb alloy was deposited using HVOF thermal spray under several spray conditions. In the present study, methane was used as a fuel gas with nitrogen. The latter was used as a powder carrier gas. Flat and tube substrates of approximate dimensions 70 mm × 25 mm × 0.8 mm thick and 22 mm × 1 mm, respectively, were coated using the following procedure. Substrate sheets were mounted on a cylindrical holder rotated at 245 rpm. The HVOF gun was placed in front of the substrates at a stand-off distance of 200 and 300 mm, to give a horizontal spray jet, and traversed vertically with a speed of 0.05 m s^{-1}. Spray parameters are shown in Table 1. A deposit thickness of about 200 μm was achieved after 20 passes of the gun. After spraying, an annealing treatment at 1073 K was carried out on samples in order to improve their magnetic properties.

2.2. Deposit characterization

In order to determine the structural state of the phase present, X-ray diffraction was performed at a scanning rate of 3° min^{-1} on samples of the as-received powder and as-sprayed coatings, using monochromatic Cu Kα radiation with a Philips X'Pert diffractometer. Samples were sectioned, polished and characterized using optical microscopy. The porosity content of freestanding coatings (3–4 mm wide and 10 mm long) was calculated using image analysis with NIH image free software. The resulting data were average of six measurements.

Magnetic measurements were performed using a hysteresismeter Bull M2000 SIIS, which enabled the hysteresis loops of the samples to be plotted and permitted the determination of coercivity and saturation magnetization.

Table 1
HVOF spray parameters

Parameter	Value
Spray gun	CDS 8944 3 psi
Oxygen gas flow rate (SLPM)	420
Methane fuel flow rate (SLPM)	**145**, 200
Nitrogen carrier gas flow rate (SLPM)	20
Powder feed rate (g min^{-1})	35
Spray distance (mm)	**200**, 300
Substrate type	Cu sheet used with air cooling system, Cu tube used with water cooling system
Coating thickness (μm)	200

Reference conditions are labelled in bold.

2.3. Statistical analysis

An artificial neural network (ANN) methodology was chosen to relate each of the process parameters to the microstructural features and magnetic properties. The calculation procedure was detailed in a previous study [11]. It consists of relating input and output parameters with the aid of a complex network of mathematical processors. Optimization is performed based on ANN training with experimental sets [12]. The advantage of such structure is related to the possibility of quantifying and predicting relationships between input and output variables, taking into account their interdependencies. Thus, a first structure was optimized to relate process parameters to microstructural features. A second structure was considered to relate the same process parameters to magnetic properties. When varying process parameters in the input of each structure, it was possible to express relationships between microstructural features and magnetic properties.

3. Results and discussion

The cross-sectional microstructure of an FeNb coating analyzed via optical microscopy is seen in Fig. 1. It can be seen that the coatings are dense, but with the presence of some porosity. The coating–substrate interface shows no gaps or cracks, which is a characteristic feature of good adhesion between the coating and the substrate.

The optical micrograph shows that the substrate surface is very irregular, and exhibits valley and reentrant features. The coating totally fills the reentrant features and follows exactly this extremely irregular surface. This is probably associated with the supersonic velocities of impact of the sprayed particles [13,14].

Moreover, it is clearly observed that the FeNb structure contains many pores, which are favorable paths for entry of oxygen and thus form oxides. In addition, the presence of several non-molten particles in the FeNb deposit is evident.

Fig. 2 shows the X-ray diffraction patterns for FeNb powder and coatings for two different cooling system. It can be

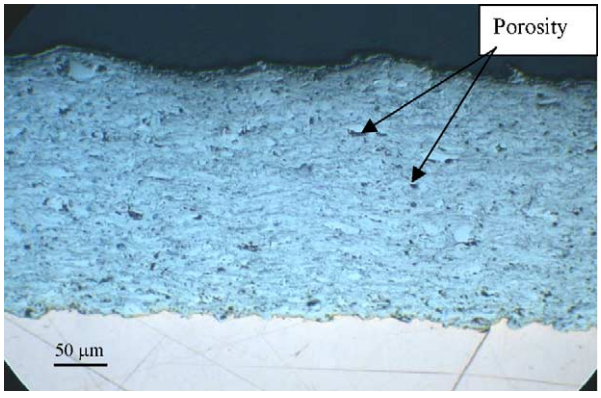

Fig. 1. Morphology of FeNb coatings.

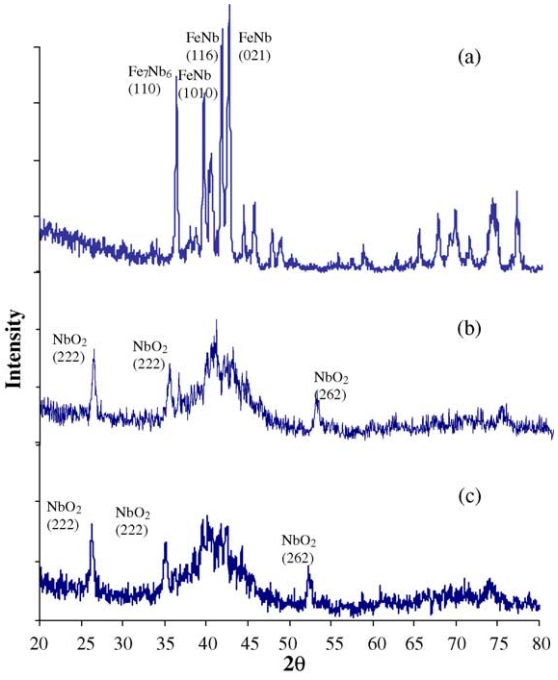

Fig. 2. X-ray diffraction patterns of FeNb samples: (a) powder, (b) coating obtained using water cooling system and (c) coating obtained using air cooling system.

seen that the structure of the coatings is partially amorphous; this amorphous phase was observed for the two modes of cooling used. The crystalline phase in the coatings has the FeNb structure, with the presence of some oxides of NbO_2. These oxides result from the use of the HVOF process though the incidence of oxidation is less marked than for the APS process [7–9].

Fig. 3 shows the predicted evolution of the porosity content with spray distance and fuel flow rate. It decreases with the increase of spray distance increases between 150 and 270 mm. However, for distances beyond 270 mm the porosity level exhibits a rapid increase. This parabolic dependence can be explained by considering particle temperature variation with

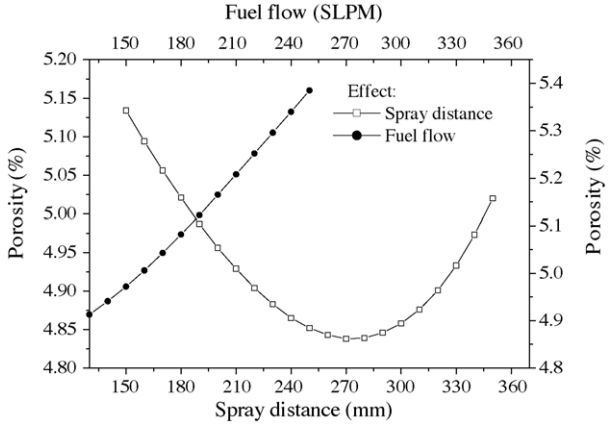

Fig. 3. Porosity level predicted evolution vs. spray distance and fuel flow rate (air cooling system).

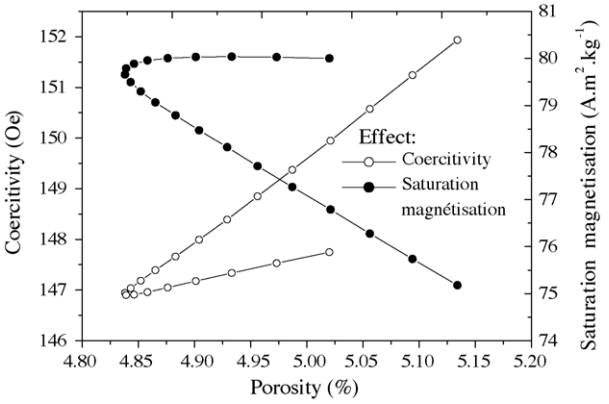

Fig. 4. Predicted evolution of coercivity and saturation magnetisation vs. porosity level.

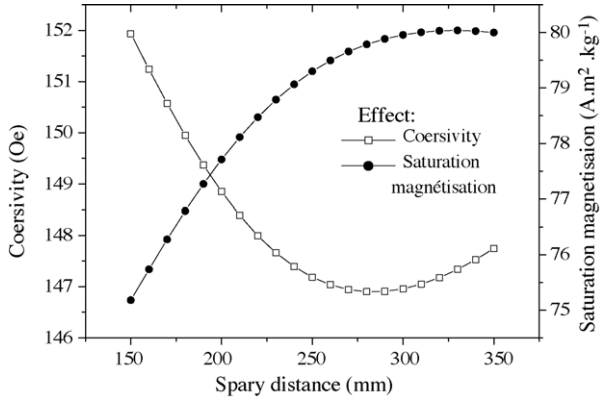

Fig. 5. Predicted evolution of coercivity and saturation magnetisation vs. spray distance (fuel flow volume = 145 SLPM, air cooling system).

respect to spray distance. For short spray distances, particle residence time is short in the flame. Consequently, they are less heated when they strike the substrate and thus cannot flatten adequately. This leads to a high porosity level in the coating [15,16]. In contrast, for large spray distances, particles leave the flame and begin to solidify before they impinge

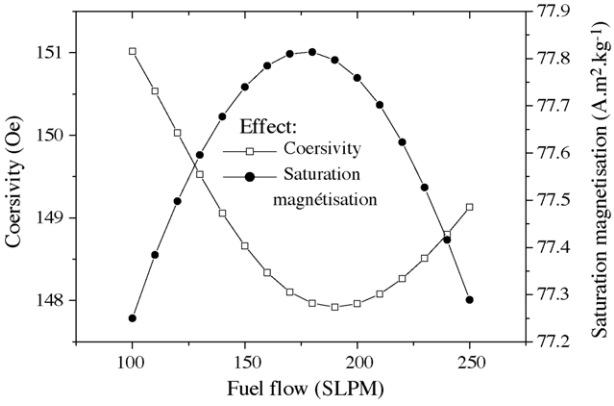

Fig. 6. Predicted evolution of coercivity and saturation magnetisation vs. fuel flow rate (spray distance = 200 mm, air cooling system).

Table 2
Measured coating porosity and magnetic properties associated to HVOF process parameters used in this study

Parameters			Characteristics		
Spray distance (mm)	Fuel flow rate (SLPM)	Cooling mode (–)	Porosity (%)	HC (Oe)	MS (A m^2 kg^{-1})
200	145	Air	4.2 ± 1.54	137 ± 21.02	75.5 ± 7.54
300	145	Air	4 ± 1.36	136 ± 20.30	76 ± 7.81
300	200	Air	4.5 ± 1.07	136 ± 20.62	75.5 ± 7.45
200	145	Water	4 ± 1.30	137 ± 20.51	75.5 ± 7.44
300	145	Water	5 ± 1.50	138 ± 19.77	75 ± 7.6
300	200	Water	4.3 ± 1.25	138 ± 19.99	75.5 ± 7.53

on the substrate. The porosity level increases consequently for the same conditions.

The variation of porosity level in the coating as a function of fuel flow is also shown in Fig. 3. This figure indicates that the porosity level shows a linear evolution with fuel flow increase. This evolution is due to the reduction of the flame temperature with increasing fuel flow rate [17]. This reduction favours the presence of the unmolten particles in the coating. In addition, for those particles that do melt their viscosity is increased such that they are unable to impact and adhere to the substrate. Generally, for low fuel flow rates, the particle velocity and temperature are associated with a low spray efficiency and consequently with degradation of magnetic properties. For high fuel flow rates, increase of particle velocity and evaporation could be related to the lowering of magnetic property values. These effects are associated with a high porosity level.

In such a way, Fig. 4 shows the coercivity and saturation magnetisation responses as a function of porosity level response. The linear increase of coercivity is explained by the fact that the porosity acts against the continuity of magnetic properties through the coating structure. These are consid-

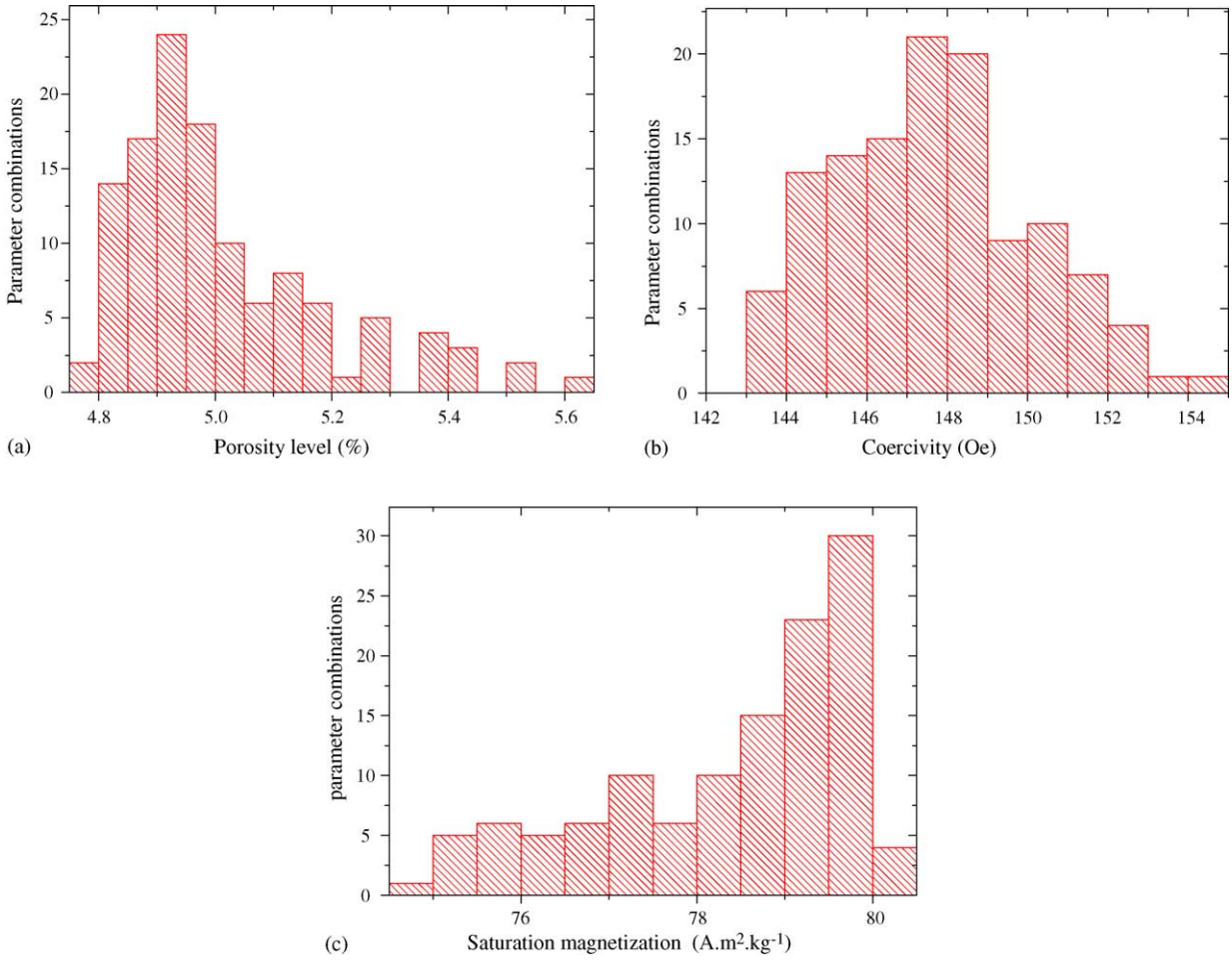

Fig. 7. Predicted network response as function of the combinations identified in the parameter space: (a) porosity, (b) coercivity and (c) magnetization saturation (air cooling system).

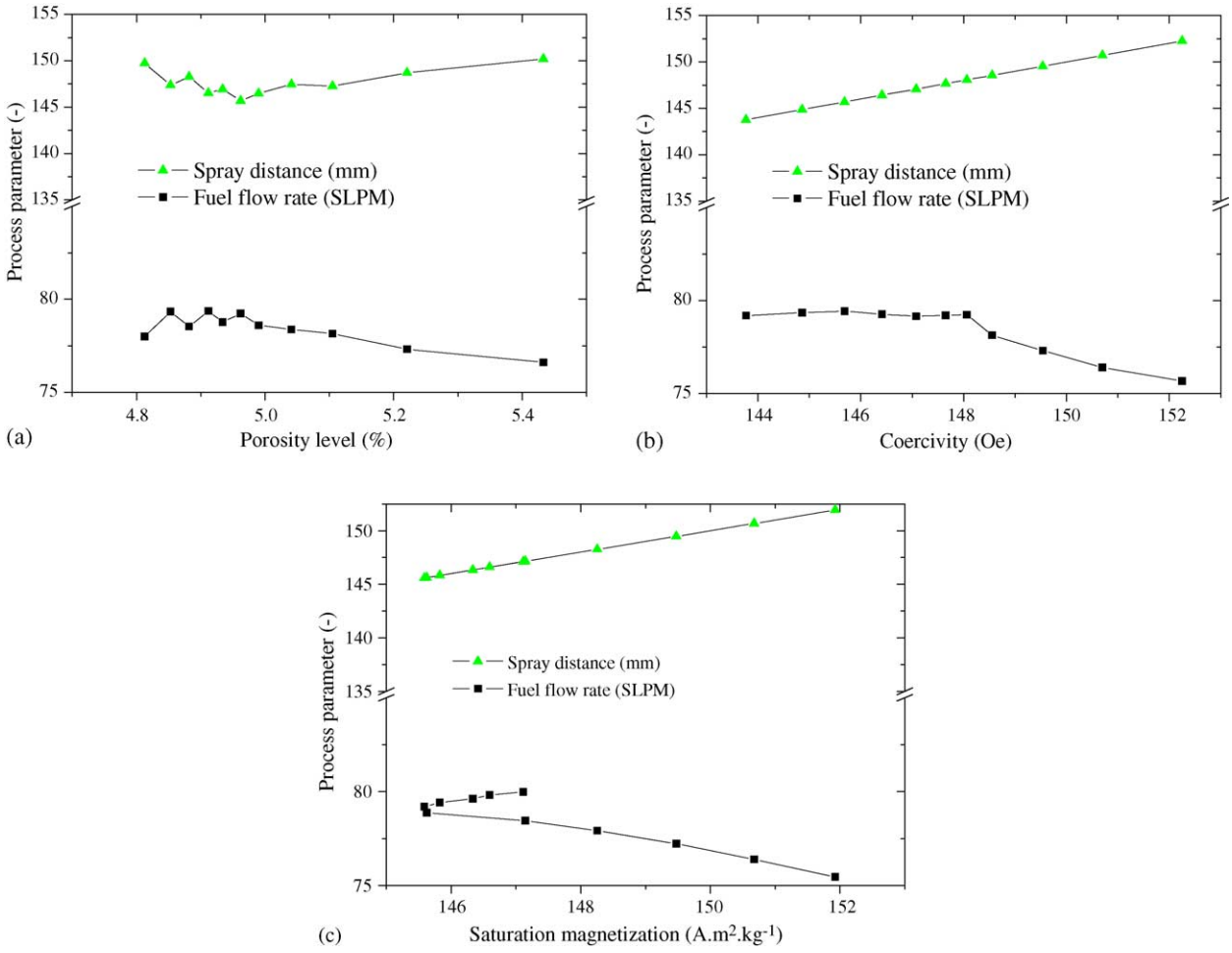

Fig. 8. Analysis of the parameter combinations by varying one parameter and selecting the possible combinations with the other studied parameters: (a) porosity, (b) coercivity and (c) saturation magnetisation (air cooling system).

ered as defects anchoring Bloch walls and involving consequently an increase of coercivity [18]. One can conclude that an improvement in coercivity can be related to low porosity content and this is obtained when spray distance is around 275 mm. This figure shows also the predicted variation of saturation magnetization as a function of porosity level. A small decrease of saturation magnetization occurs with increased porosity. Generally, in magnetism studies, the decrease of this parameter is related to coercivity increase [19].

Figs. 5 and 6 illustrate an example of predicted curves when varying the spray distance and the fuel flow at the input pattern of the second ANN. These curves show the variation of coating coercivity and saturation magnetisation with spray distance and with fuel flow rate, respectively. The same trend as for the porosity level is seen when the spray distance increases (Fig. 5). However, when the fuel flow increases, the coercivity shows a parabolic variation (Fig. 6). To explain such a correlation, one has to consider the effect of the coating porosity level as intermediate variable between the process parameters and the magnetic properties. Thus, for the same process parameter variation, the responses are calculated from the optimized ANN structures. The saturation magnetization exhibited parabolic relationships with spray distance (Fig. 5) and with fuel flow rate (Fig. 6). This could be related to particle velocity and temperature variations as in the case of coercivity.

When changing the cooling mode from the air to the water system, the magnetic properties exhibited linear variations. Such evolutions are associated to the fact that this parameter was considered as a classification variable. These results obtained by calculated method are practically in accord with our experiment results. Table 2 measured coating porosity and magnetic properties associated to HVOF process parameters were used in this study.

In order to go deeply in the statistical analysis, instead of varying individually each parameter, parameter combinations are considered. This permits to drag the parameter space with a resolution of at least 11 points for each parameter. The total number of combinations is thus 121. Fig. 7 shows the histogram representing the frequency of parameter combinations for a given value of porosity, coercivity and saturation magnetization. Overlay, these responses are predicted to vary between 4.79 and 5.63%; 143 and 154 Oe; 75 and 80 A m^2 kg^{-1}.

The analysis of the results of the parameter combinations permits also to predict the average variation of the magnetic properties and porosity with respect to each process parameter whatever are the values of the other parameters. To do so, the predicted responses are averaged for a fixed value of the process parameter. This analysis permits to confirm and generalize the parameter effects identified by varying each parameter individually and fixing the other parameters to an arbitrary value. Fig. 8 shows the evolution of the predicted responses as function of the studied parameters.

4. Summary and conclusions

The study examined the effect of HVOF thermal spraying parameters on the microstructure and magnetic properties of coatings using artificial neural network methodology:

(a) Our preliminary results showed that FeNb alloys are partially amorphous with a paramagnetic structure. After crystallization by heat treatment, the magnetic properties of the FeNb were weakly improved.
(b) Predicted results show that spray distance and fuel flow modified the deposit porosity. A decrease resulted in improvement of coercivity and saturation magnetization.

References

[1] W.L. Johnson, ASM Metals Handbook, vol. 2, 10th ed., ASM International, Metals Park, Ohio, USA, 1990, p. 804.
[2] R.W. Cahn, in: R.W. Cahn, P. Haasen, E.J. Kramer (Eds.), Materials Science and Technology, vol. 9, VCH, Weinheim, Germany, 1991, p. 494.
[3] K. Hashimoto, in: H.H. Lieberman (Ed.), Rapidly Solidified Alloys—Processes, Structures, Properties and Applications, Marcel Dekker, New York, 1993, p. 591.
[4] S.K. Das, E.M. Norin, R.L. Bye, in: B.H. Kear, B.C. Giessen (Eds.), Proceedings of the Materials Research Society Symposium, vol. 28, Materials Research Society, Pittsburgh, PA, USA, 1984, p. 233.
[5] C. Moreau, P. Cielo, M. Lamontagne, S. Dallaire, J.C. Krapez, M. Vardelle, Surf. Coat. Technol. 46 (1991) 173.
[6] R.W. Smith, R. Knight, J. Met. 47 (8) (1995) 32.
[7] N.E. Feninechе, M. Cherigui, A. Kellou, H. Aourag, C. Coddet, in: R. Marple, C. Moreau (Eds.), Advancing the Science and Applying the Technology, ASM International, Materials Park, OH, USA, 2003, p. 1409.
[8] N.E. Feninechе, M. Cherigui, H. Aourag, C. Coddet, Mater. Lett. 58 (2004) 1797.
[9] M. Cherigui, H.I. Feraoun, N.E. Feninechе, H. Aourag, C. Coddet, Mater. Chem. Phys. 85 (2004) 113.
[10] S.R. Kim, S.H. Lim, J. Alloys Compd. 258 (1997) 163.
[11] M. Cherigui, S. Guessasma, N.E. Feninechе, C. Coddet, Mater. Sci. Eng. B 166 (2005) 40.
[12] T. Sahraoui, S. Guessasma, N.E. Feninechе, G. Montavon, C. Coddet, Mater. Lett. 58 (2004) 654.
[13] D.L. Gilmore, R.C. Dykhuizen, R.A. Neiser, T.J. Roemer, M.F. Smith, J. Thermal Spray Technol. 8 (4) (1999) 576.
[14] R.S. Lima, J. Karthikeyan, C.M. Kay, J. Lindemann, C.C. Berndt, Thin Solid Films 416 (2002) 129.
[15] V.V. Sobolev, J.M. Guilemany, Mater. Lett. 18 (1994) 304.
[16] L. Zhao, M. Parco, E. Lugscheider, Surf. Coat. Technol. 184 (2004) 298.
[17] B.R. Marple, J. Voyer, J.-F. Bisson, C. Moreau, J. Mater. Process. Technol. 117 (2001) 418.
[18] M. Nacken, W. Heller, Arch. Eisenhuettenw. 31 (1961) 153.
[19] R.M. Bozorth, H.J. Williams, Rev. Mod. Phys. 17 (1945) 72.